ELSEVIER

Journal of Nuclear Materials 302 (2002) 41–48

journal of nuclear materials

www.elsevier.com/locate/jnucmat

Modeling hydrogen and helium entrapment in flowing liquid metal surfaces as plasma-facing components in fusion devices

Ahmed Hassanein *

Argonne National Laboratory, 9700 South Cass Avenue, Argonne, IL 60439, USA

Received 12 November 2001; accepted 21 December 2001

Abstract

In a fusion reactor, the ability to use liquids as plasma-facing components (PFCs) depends on their interaction with the plasma and the magnetic field. One important issue for the moving liquid is the ability to entrain particles that strike the PFC surface (helium and hydrogen isotopes) while accommodating high heat loads. To study this problem, an analytical model and a two-dimensional comprehensive numerical model have been developed and implemented in the HEIGHTS computer simulation package. The models take into account the kinetics of particle injection, motion and interactions with the liquid lattice, and the ultimate release from the surface. The models were used to investigate an important issue, whether He particles can be pumped by the PFC liquid rather than requiring a standard vacuum system. Hydrogen isotope (DT) particles that strike the surface will likely be trapped in the liquid–metal surface (e.g., lithium) due to the high chemical solubility of hydrogen. The impinging He particles in the established low-recycling regime at PFCs could be harder to pump using the standard vacuum pumping techniques. The analysis results indicate a reasonable chance of adequate helium self-trapping in flowing lithium as PFC without active pumping. © 2002 Published by Elsevier Science B.V.

1. Introduction

One of the most challenging areas for fusion power production in a tokamak device is the development of plasma-facing components (PFCs) that can withstand high heat and particle fluxes during normal and abnormal events. Renewable liquid metal surfaces offer significant advantages over the standard solid components. However, the ability to use liquids as divertor surfaces depends on their interaction with the plasma and the reactor's strong magnetic field. One important issue that will influence the selection of liquid surfaces is whether the moving liquid will entrain particles that strike the surface while still accommodating high heat loads. Particle entrapment, in particular, could determine the viability of specific liquid candidates as renewable divertor surfaces. Hydrogen isotope (DT) particles striking the surface will most likely be trapped in the lithium surface because of the high chemical solubility of the hydrogen in liquid lithium. This will result in a low-recycling divertor and a high edge temperature (several hundred electron volt) [1].

There are several implications of a low-recycling divertor on plasma performance. An important issue is whether He can be pumped at low density by a standard vacuum system. If helium particles are not entrained in the surface and must be pumped out of the divertor, then standard vacuum pumping techniques must be used. However, the low-recycling regime also results in a low density and pressure at the pump ducts. Because helium is a difficult species to vacuum pump, it may be

* Tel.: +1-630 252 5889; fax: +1-630 252 5287.
E-mail address: hassanein@anl.gov (A. Hassanein).

0022-3115/02/$ - see front matter © 2002 Published by Elsevier Science B.V.
PII: S0022-3115(02)00726-2

more difficult or impossible to obtain adequate pumping in this situation.

The potential for any of the liquid candidates (e.g., Li, Sn, Ga, flibe) to work satisfactorily depends on whether particles with negligible chemical solubility (for example, He in Li and DT in flibe) become entrained in the surface for a long enough time to be removed from the divertor chamber. If He is entrained in lithium and so removed, the lithium system would eliminate the need for separate vacuum pumping and, therefore, would become more attractive. On the other hand, complete recycling (little or no entrapment) would make He removal from the lithium system difficult or impossible.

The overall understanding of particle dynamic entrapment in liquid surfaces is crucial to assessing their viability for divertor operation. The purpose of this study is to investigate whether a liquid lithium layer will pump/absorb the incoming flux of helium, deuterium, and tritium. The kinetics of particle penetration, motion, and interactions with the liquid lattice, along with the ultimate release from the surface, are modeled in this analysis. Two models, an analytical and a numerical one, are developed in this study. The analytical model offers a quick assessment of He removal efficiency as a function of system parameters of both the incident He particles and the flowing liquid–metal surface. The integrated numerical model is more general, with a wide range of applications and various boundary conditions. The numerical model is implemented with the HEIGHTS package [2], which takes into account the kinetics of particle injection, motion, interactions with the liquid lattice, and the ultimate release from the moving surface.

Formation and growth of trapped gas bubbles near the surface layer of the liquid metal can lead to bubble explosion and ejection/sputtering of macroscopic droplets. The possible effects of macroscopic droplet erosion on the scrape-off-layer (SOL) plasma and overall reactor operation are briefly discussed.

2. Helium pumping requirement in the liquid

Helium ash produced from the thermonuclear reaction in a fusion reactor needs to be removed at its production rate. For example, in a 2000-MW fusion power reactor operating in the low-recycle regime, the alpha-production rate $I_{\mathrm{Fus}} = 2000$ MW/(17.6 MeV/fusion) $\approx 7.1 \times 10^{20}$ He/s. For a DT current to the divertor, $I_{\mathrm{DT}} \approx 1.6 \times 10^{23}$ s^{-1}, and for the 10% He/(D+T) fraction in the core plasma, the helium current to the divertor is $I_{\mathrm{He}} \approx 1.6 \times 10^{22}$ s^{-1}. Therefore, the required removal efficiency is $\varepsilon = I_{\mathrm{Fus}}/I_{\mathrm{He}} \approx 0.04$, or $\approx 5\%$. Recent studies, however, suggest that the He removal rate could be $<5\%$ [3].

3. Computational models

The development of a model describing absorption of helium and deuterium–tritium particles by a layer of liquid metal entails solving a time-independent, two-dimensional diffusion equation in the x–y poloidal plane, schematically illustrated in Fig. 1, with various boundary conditions.

3.1. Simple analytical model for He pumping

The absorption of He plasma particles by a layer of liquid metal can be described by solving the general diffusion equation:

$$\begin{aligned} &v_0 \frac{\partial c}{\partial y} = D \frac{\partial^2 c}{\partial x^2} + q\delta(x - l), \quad x \geqslant 0, \;\; y = 0, L \\ &c(x = 0, y) = 0 \\ &c(x, y = 0) = 0, \end{aligned} \tag{1}$$

where $c(x, y)$ is He concentration in depth x along flow distance y, D is diffusion coefficient, v_0 is velocity of liquid layer, L is total exposed length of liquid layer, l is thickness of particle absorption zone, and q is incident He particle flux. The incident He flux is assumed to be implanted at a definite range $x = l$, as described by the δ function given in Eq. (1). The distance l is the projected range estimated from the incident He particle energy.

The following substitution is made into Eq. (1):

$$c = c_0 c', \quad y = l y', \quad x = l x'. \tag{2}$$

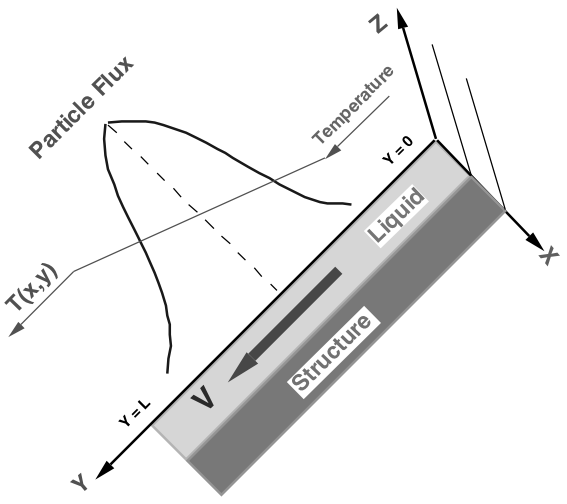

Fig. 1. Schematic illustration of particle interaction with free liquid surface.

In dimensionless variables Eq. (1) is then written as

$$\frac{\partial c}{\partial y} = \frac{D}{v_0 l}\frac{\partial^2 c}{\partial x^2} + \frac{lq}{v_0 c_0}\delta(x-1), \quad x \geqslant 0, \;\; y = 0, \frac{L}{l}. \tag{3}$$

Let's introduce the dimensionless parameters:

$$a = \frac{D}{v_0 l}, \quad \lambda = \frac{l}{L}, \quad \text{and} \quad \bar{q} = \frac{lq}{v_0 c_0}. \tag{4}$$

Then, Eq. (3) can be written as

$$\frac{\partial c}{\partial y} = a\frac{\partial^2 c}{\partial x^2} + \bar{q}\delta(x-1), \quad x \geqslant 0, \;\; y = 0, \frac{1}{\lambda}. \tag{5}$$

In this system of equations, the problem has an analytical solution that can be expressed using Green's function:

$$c(x,y) = \frac{\bar{q}}{2\sqrt{a\pi}}\int_0^y \int_0^\infty \frac{\delta(\xi-1)}{\sqrt{y-\eta}}\left[\exp\left(-\frac{(x-\xi)^2}{4a(y-\eta)}\right) - \exp\left(-\frac{(x+\xi)^2}{4a(y-\eta)}\right)\right]\mathrm{d}\xi\,\mathrm{d}\eta. \tag{6}$$

The integral on the δ function gives

$$c(x,y) = \frac{\bar{q}}{2\sqrt{a\pi}}\int_0^y \frac{1}{\sqrt{y-\eta}}\left[\exp\left(-\frac{(x-1)^2}{4a(y-\eta)}\right) - \exp\left(-\frac{(x+1)^2}{4a(y-\eta)}\right)\right]\mathrm{d}\eta. \tag{7}$$

Let's now introduce two new variables:

$$X_\pm = \frac{x \pm 1}{2\sqrt{a}}. \tag{8}$$

Then, we may rewrite Eq. (7) as

$$c(x,y) = \frac{\bar{q}}{2\sqrt{a\pi}}\int_0^y \frac{1}{\sqrt{y-\eta}}\left[\exp\left(-\frac{X_-^2}{(y-\eta)}\right) - \exp\left(-\frac{X_+^2}{(y-\eta)}\right)\right]\mathrm{d}\eta. \tag{9}$$

Further

$$\int_0^y \frac{1}{\sqrt{y-\eta}}\exp\left(-\frac{X_\pm^2}{(y-\eta)}\right)\mathrm{d}\eta = I_\pm. \tag{10}$$

Substituting in the last integral

$$\begin{aligned}\beta &= \sqrt{\frac{X_\pm^2}{y-\eta}}\\ \mathrm{d}\beta &= \frac{|X_\pm|}{2}\frac{\mathrm{d}\eta}{(y-\eta)^{3/2}} = \frac{\beta^3}{2X_\pm^2}\mathrm{d}\eta\\ \mathrm{d}\eta &= \frac{2X_\pm^2}{\beta^3}\mathrm{d}\beta\end{aligned} \tag{11}$$

gives

$$\begin{aligned} I_\pm &= 2|X_\pm|\int_{|X_\pm|/\sqrt{y}}^\infty \frac{\exp(-\beta^2)}{\beta^2}\mathrm{d}\beta\\ &= -2|X_\pm|\int_{|X_\pm|/\sqrt{y}}^\infty \exp(-\beta^2)\mathrm{d}\left(\frac{1}{\beta}\right)\\ &= -2|X_\pm|\left(\exp(-\beta^2)\frac{1}{\beta}\Big|_{|X_\pm|/\sqrt{y}}^\infty + 2\int_{|X_\pm|/\sqrt{y}}^\infty \exp(-\beta^2)\mathrm{d}\beta\right)\\ &= 2|X_\pm|\left(\exp\left(-\frac{X_\pm^2}{y}\right)\frac{\sqrt{y}}{|X_\pm|} - \sqrt{\pi}\,\mathrm{erfc}\left(\sqrt{\frac{X_\pm^2}{y}}\right)\right)\\ &= 2\left(\exp\left(-\frac{X_\pm^2}{y}\right)\sqrt{y} - \sqrt{\pi}|X_\pm|\,\mathrm{erfc}\left(\sqrt{\frac{X_\pm^2}{y}}\right)\right). \end{aligned} \tag{12}$$

Using Eq. (12), one can then write

$$\begin{aligned} c(x,y) &= \frac{\bar{q}}{2\sqrt{a\pi}}(I_- - I_+)\\ &= \frac{\bar{q}}{2\sqrt{a\pi}}\left(2\left(\exp\left(-\frac{X_-^2}{y}\right)\sqrt{y} - \sqrt{\pi}|X_-|\,\mathrm{erfc}\left(\sqrt{\frac{X_-^2}{y}}\right)\right) - 2\left(\exp\left(-\frac{X_+^2}{y}\right)\sqrt{y} - \sqrt{\pi}|X_+|\,\mathrm{erfc}\left(\sqrt{\frac{X_+^2}{y}}\right)\right)\right)\\ &= \frac{\bar{q}}{\sqrt{a\pi}}\left(\sqrt{y}\left(\exp\left(-\frac{X_-^2}{y}\right) - \exp\left(-\frac{X_+^2}{y}\right)\right) - \sqrt{\pi}\left(|X_-|\,\mathrm{erfc}\left(\sqrt{\frac{X_-^2}{y}}\right) - |X_+|\left(\sqrt{\frac{X_+^2}{y}}\right)\right)\right). \end{aligned} \tag{13}$$

The amount of particles carried away (i.e., pumped) by the moving liquid metal per unit time is defined by

$$Q_{\text{pump}} = \int_0^\infty c\left(x, y = \frac{1}{\lambda}\right)\mathrm{d}x. \tag{14}$$

The total amount of absorbed He particles is then given by

$$Q_{\text{all}} = \bar{q}\int_0^{1/\lambda}\int_0^\infty \delta(x-1)\,\mathrm{d}x\,\mathrm{d}y = \frac{\bar{q}}{\lambda}. \tag{15}$$

The pumping coefficient (ratio of He removal) is defined as

$$\xi = \frac{Q_{\text{pump}}}{Q_{\text{all}}} = \frac{\lambda}{\bar{q}}\int_0^\infty c\left(x, y = \frac{1}{\lambda}\right)\mathrm{d}x. \tag{16}$$

Then

$$
\begin{aligned}
Q_{\text{pump}} &= \int_0^\infty c\left(x, y=\frac{1}{\lambda}\right)\mathrm{d}x \\
&= \frac{\bar{q}}{2\sqrt{a\pi}} \int_0^{1/\lambda} \frac{1}{\sqrt{1/\lambda-\eta}} \int_0^\infty \left[\exp\left(-\frac{X_-^2}{(1/\lambda-\eta)}\right)\right. \\
&\quad \left. - \exp\left(-\frac{X_+^2}{(1/\lambda-\eta)}\right)\right]\mathrm{d}x\,\mathrm{d}\eta \\
&= \frac{\bar{q}}{2\sqrt{a\pi}} \int_0^{1/\lambda} \frac{1}{\sqrt{1/\lambda-\eta}} \int_0^\infty \left[\exp\left(-\frac{(x-1)^2}{4a(1/\lambda-\eta)}\right)\right. \\
&\quad \left. - \exp\left(-\frac{(x+1)^2}{4a(1/\lambda-\eta)}\right)\right]\mathrm{d}x\,\mathrm{d}\eta \\
&= \frac{\bar{q}}{2} \int_0^{1/\lambda} \left(\mathrm{erfc}\left(-\frac{1}{2\sqrt{a(1/\lambda-\eta)}}\right)\right. \\
&\quad \left. - \mathrm{erfc}\left(\frac{1}{2\sqrt{a(1/\lambda-\eta)}}\right)\right)\mathrm{d}\eta \\
&= \bar{q} \int_0^{1/\lambda} \mathrm{erf}\left(\frac{1}{2\sqrt{a(1/\lambda-\eta)}}\right)\mathrm{d}\eta \\
&= \frac{\bar{q}}{2a} \int_{\frac{1}{2}\sqrt{\lambda/a}}^\infty \mathrm{erf}(\beta)\frac{1}{\beta^3}\mathrm{d}\beta. \qquad (17)
\end{aligned}
$$

Therefore, the pumping coefficient is

$$
\xi = \frac{1}{2}\frac{\lambda}{a}\int_{\frac{1}{2}\sqrt{\lambda/a}}^\infty \frac{\mathrm{erf}(\beta)}{\beta^3}\mathrm{d}\beta. \qquad (18)
$$

Let's define a pumping parameter S as

$$
S = \frac{1}{2}\sqrt{\frac{\lambda}{a}} = \frac{1}{2}\sqrt{\frac{l^2 v_0}{DL}}. \qquad (19)
$$

Then, the particle pumping coefficient can be expressed as

$$
\xi = 2S^2 \int_s^\infty \frac{\mathrm{erf}(\beta)}{\beta^3}\mathrm{d}\beta. \qquad (20)
$$

Further

$$
\begin{aligned}
\int_s^\infty \frac{\mathrm{erf}(\beta)}{\beta^3}\mathrm{d}\beta &= -\frac{1}{2}\int_s^\infty \mathrm{erf}(\beta)\mathrm{d}\left(\frac{1}{\beta^2}\right) \\
&= -\frac{1}{2}\left(\mathrm{erf}(\beta)\frac{1}{\beta^2}\Big|_s^\infty - \int_s^\infty \frac{1}{\beta^2}\mathrm{d}(\mathrm{erf}(\beta))\right) \\
&= \mathrm{erf}(S)\frac{1}{2S^2} + \frac{1}{\sqrt{\pi}}\exp(-S^2)\frac{1}{S} - (1-\mathrm{erf}(S)) \\
&= \mathrm{erf}(S)\left(\frac{1}{2S^2}+1\right) + \frac{1}{\sqrt{\pi}}\exp\left(-S^2\right)\frac{1}{S} - 1. \qquad (21)
\end{aligned}
$$

And finally

$$
\xi = \mathrm{erf}(S)(1+2S^2) + \frac{2S}{\sqrt{\pi}}\exp(-S^2) - 2S^2. \qquad (22)
$$

For typical reactor system parameters of $l \approx 10^{-8}$–10^{-6} m, $v_0 \approx 10$ m/s, $D \approx 10^{-10}$–10^{-8} m^2/s, and $L \approx 0.1$ m, the pumping parameter $S \ll 1$. Then

$$
\xi \approx 2S \approx \sqrt{\frac{\lambda}{a}} = \sqrt{\frac{l^2 v_0}{DL}}. \qquad (23)
$$

For helium pumping, the value of $\xi \approx 10^{-3}$–10^{-2} is small and is in the order of ≈1%. Fig. 2 shows the dependence of the He pumping coefficient ξ on the pumping parameter for a wide range of S.

The calculated value of ξ is very small and is in the same order as the desired He removal rate (few percent needed for the self-pumping) for reasonable operating pumping parameters of a typical liquid–metal divertor surface. Therefore, more precise values of ξ, require a detailed numerical calculation which takes into account an accurate particle implantation spatial profile, the temperature dependence of material properties, and different boundary conditions.

3.2. General numerical model

A self-consistent and integrated numerical model for the kinetics of particle injection, motion and interactions with the liquid lattice, and the ultimate release from the surface has been developed and implemented using the HEIGHTS package [2]. This model is summarized below.

The basic general equation can be written as

$$
\begin{aligned}
v_0\frac{\partial c(x,y)}{\partial y} &= -\frac{\partial}{\partial x}J(x,y) - Q_0 Q(x,y)c(x,y) \\
&\quad + G_0 G(x,y,l_0), \quad 0 \leqslant x \leqslant L_x, \quad 0 \leqslant y \leqslant L_y, \qquad (24)
\end{aligned}
$$

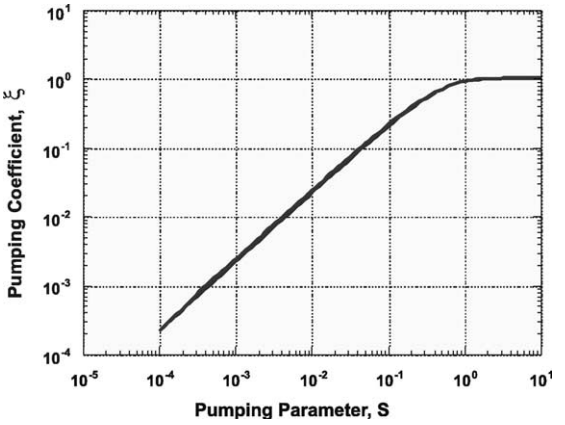

Fig. 2. Helium pumping coefficient as a function of the pumping parameter.

where $c(x,y)$ is again particle concentration at depth x along flow distance y, v_0 is liquid moving velocity, l_0 is maximum particle implantation depth, L_x is depth of the liquid layer, and L_y is exposed length of liquid surface to the plasma as illustrated in Fig. 1. The functions $Q(x,y)$ and $G(x,y)$ are for particle absorption and implantation fluxes, respectively. The flux, J, is determined as follows:

$$J(x,y) = -D_0 D(T(x,y)) \frac{\partial c(x,y)}{\partial x}. \tag{25}$$

The values D_0, Q_0, and G_0 are dimensional constants that characterize the rates of diffusion, absorption, and implantation, respectively.

The boundary condition is

$$c(x,0) = c_0(x), \tag{26}$$

where usually $c_0(x) = 0$. Two kinds of boundary condition are considered at the surface. The first is

$$c(0,y) = 0, \tag{27}$$

where zero surface concentration is assumed for the helium implantation case. The second boundary condition,

$$D\frac{\partial}{\partial x} c(0,y) = K_r c^2(0,y), \tag{28}$$

predicts the surface recombination of a diatomic molecule (for D_2 and T_2), where the molecular recombination constant K_r can be calculated in various ways [4–6], for example [6]:

$$K_r(T) = \frac{4\alpha c_1 \exp\left[(2E_s - E_x)/kT\right]}{\rho\sqrt{MT}S_0^2}, \tag{29}$$

where α is a sticking coefficient, c_1 is a constant, k is Boltzmann's constant, T is temperature, ρ is density, and M is hydrogen isotope atomic mass. The solubility, S, is the concentration of deuterium and tritium atoms in the target material that is in equilibrium with DT gas at a pressure P given by

$$S(T,P) = S_0\sqrt{P}\exp(-E_s/kT), \tag{30}$$

where S_0 is a material constant, and E_s is the heat of solution, which can be either positive (endothermic) or negative (exothermic), indicating that energy is either expended or liberated when hydrogen is absorbed into material. Various formulas for surface recombination rates did not significantly change the results of this study.

The particle diffusivity D is a measure of particle mobility in the liquid and generally has the form

$$D = D_0 \exp(-E_d/kT), \tag{31}$$

where D_0 is a material constant, and E_d is the migration energy. The surface barrier E_x in Eq. (29) is given by [6]

$$E_x = \max(E_s + E_d, 0). \tag{32}$$

By substitution of

$$x = l_0 x' \quad \text{and} \quad y = y'\frac{v_0 l_0^2}{D_0}, \tag{33}$$

Eq. (24) can then be written as

$$\frac{\partial c(x,y)}{\partial y} = -\frac{\partial}{\partial x} J(x,y) - q_0 Q(x,y)c(x,y) + g_0 G(x,y),$$
$$0 \leqslant x \leqslant \frac{L_x}{l_0}, \quad 0 \leqslant y \leqslant \frac{L_y D_0}{l_0^2 v_0} \equiv L, \quad q_0 = \frac{Q_0 l_0^2}{D_0}, \quad g_0 = \frac{G_0 l_0^2}{D_0}, \tag{34}$$

where

$$J(x,y) = -D(T(x,y))\frac{\partial c(x,y)}{\partial x}. \tag{35}$$

We have used the integral–interpolating method to solve this parabolic equation and obtain an accurate numerical solution. This method is briefly described below.

We introduce non-uniform mesh and grid functions as follows:

$$\left\{\begin{array}{l} x_i, \quad i = 0,1,\ldots,M; \quad x_0 = 0, \quad x_N = L_x/l_0; \\ \quad x_{i+1/2} = \frac{x_{i+1}+x_i}{2}; \quad h_i = x_{i+1} - x_i \\ y_n = \tau n; \quad n = 0,1,2\ldots N; \quad \tau = L/N \end{array}\right\} \tag{36}$$
$$\left\{f_i^n = f(x_i,y_n); \quad f_{i+1/2}^n = f\left(x_{i+1/2},y_n\right)\right\}.$$

Integrating Eq. (34) on each cell, one obtains

$$\begin{aligned}\int_{y_n}^{y_{n+1}}\int_{x_{i-1/2}}^{x_{i+1/2}} \frac{\partial c(x,y)}{\partial y}\mathrm{d}x\,\mathrm{d}y &= -\int_{y_n}^{y_{n+1}}\int_{x_{i-1/2}}^{x_{i+1/2}} \frac{\partial}{\partial x} J(x,y)\mathrm{d}x\,\mathrm{d}y \\ &\quad - q_0\int_{y_n}^{y_{n+1}}\int_{x_{i-1/2}}^{x_{i+1/2}} Q(x,y)c(x,y)\mathrm{d}x\,\mathrm{d}y \\ &\quad + g_0\int_{y_n}^{y_{n+1}}\int_{x_{i-1/2}}^{x_{i+1/2}} G(x,y)\mathrm{d}x\,\mathrm{d}y \end{aligned} \tag{37}$$

and

$$\begin{aligned}\int_{x_{i-1/2}}^{x_{i+1/2}} c(x,y_n)\mathrm{d}x - \int_{x_{i-1/2}}^{x_{i+1/2}} c(x,y_{n+1})\mathrm{d}x &= \int_{y_n}^{y_{n+1}} J(x_{i-1/2},y)\mathrm{d}y - \int_{y_n}^{y_{n+1}} J\left(x_{i+1/2},y\right)\mathrm{d}y \\ &\quad - q_0\int_{y_n}^{y_{n+1}}\int_{x_{i-1/2}}^{x_{i+1/2}} Q(x,y)c(x,y)\mathrm{d}x\,\mathrm{d}y \\ &\quad + g_0\int_{y_n}^{y_{n+1}}\int_{x_{i-1/2}}^{x_{i+1/2}} G(x,y)\mathrm{d}x\,\mathrm{d}y. \end{aligned} \tag{38}$$

The flux J can then be approximated as

$$J(x_{i-1/2},y) \approx -D(x_{i-1/2},y)\frac{c(x_i,y)-c(x_{i-1},y)}{h_{i-1}}$$
$$J(x_{i+1/2},y) \approx -D(x_{i+1/2},y)\frac{c(x_{i+1},y)-c(x_i,y)}{h_i}. \quad (39)$$

Therefore,

$$\begin{aligned}\int_{x_{i-1/2}}^{x_{i+1/2}} c(x,y_n)\mathrm{d}x &= \int_{x_{i-1/2}}^{x_i} c(x,y_n)\mathrm{d}x \\ &\quad + \int_{x_i}^{x_{i+1/2}} c(x,y_n)\mathrm{d}x \\ &\approx \frac{h_{i-1}}{8}(c(x_{i-1},y_n)+3c(x_i,y_n)) \\ &\quad + \frac{h_i}{8}(c(x_{i+1},y_n)+3c(x_i,y_n)) \\ &= \frac{h_{i-1}}{8}c_{i-1}^n + \frac{3(h_{i-1}+h_i)}{8}c_i^n \\ &\quad + \frac{h_i}{8}c_{i+1}^n \end{aligned} \quad (40)$$

and

$$\int_{x_{i-1/2}}^{x_{i+1/2}} c(x,y_{n+1})\mathrm{d}x = \frac{h_{i-1}}{8}c_{i-1}^{n+1} + \frac{3(h_{i-1}+h_i)}{8}c_i^{n+1} + \frac{h_i}{8}c_{i+1}^{n+1}. \quad (41)$$

The integral of J can be approximated as follows:

$$\begin{aligned}\int_{y_n}^{y_{n+1}} J(x_{i-1/2},y)\mathrm{d}y &\approx -\frac{1}{h_i}\int_{y_n}^{y_{n+1}} D(x_{i-1/2},y)(c(x_i,y) \\ &\quad - c(x_{i-1},y))\mathrm{d}y \\ &\approx -\frac{\tau}{h_{i-1}}(1-\sigma)D(x_{i-1/2},y_n)(c(x_i,y_n) \\ &\quad - c(x_{i-1},y_n)) \\ &\quad - \frac{\tau}{h_{i-1}}\sigma D(x_{i-1/2},y_{n+1})(c(x_i,y_{n+1}) \\ &\quad - c(x_{i-1},y_{n+1})) \\ &= -\frac{\tau}{h_{i-1}}\Big[(1-\sigma)D_{i-1/2}^n(c_i^n - c_{i-1}^n) \\ &\quad + \sigma D_{i-1/2}^{n+1}(c_i^{n+1} - c_{i-1}^{n+1})\Big], \end{aligned} \quad (42)$$

where $0 \leqslant \sigma \leqslant 1$ and $\sigma = 0$ in the explicit scheme, $\sigma = 1$ in the implicit scheme, and $\sigma = 0.5$ in the Crank–Nicholson scheme. The resulting set of equations is then solved separately for the helium and hydrogen isotopes by using the relevant boundary conditions.

The self-consistent modeling of the kinetics of particle injection, motion, and interactions with the liquid lattice, along with the ultimate release from the surface, is coupled with a particle implantation function. The details of the implantation of the incident helium and hydrogen isotopes in the near surface layer of liquid Li as plasma-facing material are calculated by using the 3-D ITMC Monte Carlo code, which is part of the HEIGHTS package [7]. The mesh size of the implantation zone can be as small as one monolayer thick to accurately predict the effect of the near surface area. The particle incident energies are governed by the plasma temperature in the SOL and by the sheath potential at the wall surface. Fig. 3 shows the calculated He implantation profile as a function of the incident He particle energy. These results are fitted and used in the implantation function $G(x,y)$ in Eq. (34).

The incident particle energy is determined by a number of factors, including the interaction of the sound-speed flow, He and DT equilibration, and sheath potential acceleration. Higher incident energies than 10 keV will help trap more He particles in the moving Li due to the deeper implantation. Higher particle energies are expected due to the resulting low-recycling and high-temperature operating regime of the moving-liquid metal surfaces.

The TRICS code (part of HEIGHTS) then calculates the helium and hydrogen isotope diffusion motion, trapping (if any), and surface release in the form of molecules (D_2 and T_2) due to the recombination mechanism [8]. The pumping/removal coefficient, ξ, is again defined as the ratio of the particle current removed by the flowing Li to the incident particle current from the SOL.

Fig. 4 shows the He pumping coefficient calculated as a function of Li flow velocity and He diffusion coefficient for He particles with an incident energy of 1.0 keV. To achieve an adequate He removal rate (≈5% removal efficiency, as defined earlier), with a Li diffusion coeffi-

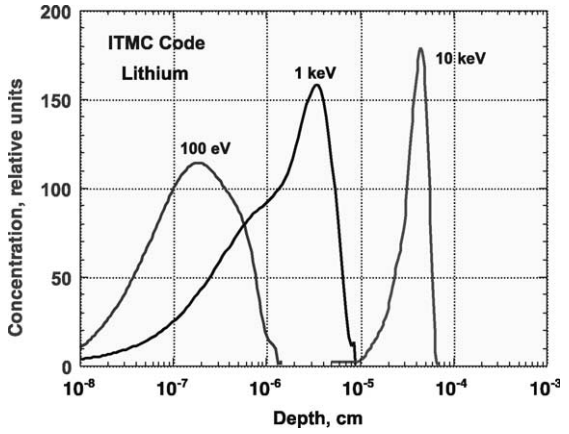

Fig. 3. Helium implantation profile in Li as a function of incident He energy.

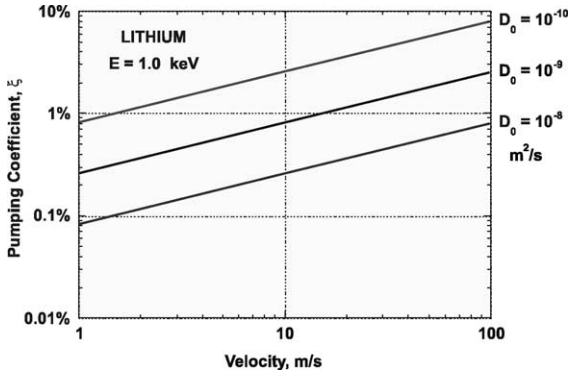

Fig. 4. HEIGHTS calculations of He pumping coefficient as a function of Li velocity at 1-keV incident particle energy.

cient of $D_0 = 10^{-10}$ m^2/s, the Li velocity should be >20–30 m/s. At higher diffusion coefficients, the required Li velocity is very high, exceeding 100 m/s. To achieve adequate He pumping at higher implantation energies (resulting from the low-recycle regime), reasonable Li velocities of ≈10 m/s could be sufficient, as shown in Fig. 5. However, if He bubbles are formed in the flowing Li near the surface layer, significant He trapping can occur. This needs more detailed investigation.

Although the range of the implanted hydrogen isotopes in Li is <0.1 μm for incident particle kinetic energy as high as 1 keV, the calculated rate of surface recombination into hydrogen isotope molecules (and therefore the release rate) is very small. This rate is small mainly because of the lower recombination coefficient and the lower surface concentration due to the short residence time of the moving liquid Li (about 10 ms for an effective 10-cm particle interaction zone moving with velocity of 10 m/s) [9]. It takes a couple of minutes for a stagnant surface to build up enough surface concentration to achieve a significant recombination and release rate. Therefore, in our case of a moving liquid surface, almost all the incident hydrogen isotope is retained in the flowing Li. In addition, hydrogen isotope concentrations near the end-of-range of the implantation zone, coupled with synergistic effects of simultaneous He implantation, could promote bubble formation. This condition will further increase the hydrogen retention due to the slow diffusion of bubbles to the surface. Therefore, in a PFC of moving liquid Li under these conditions, the Li will pump most of the incident particle flux of the hydrogen isotope and should have notable effects on the physics of the boundary layer in fusion reactors using free surface flow of liquid metals.

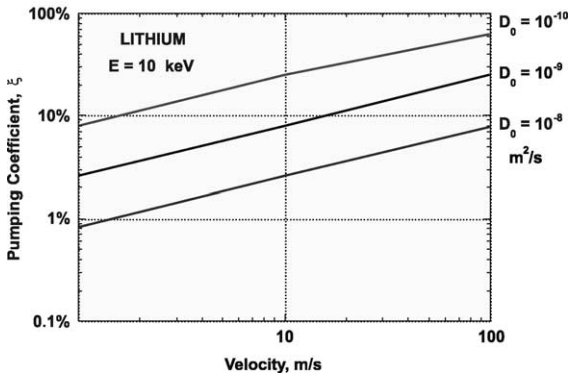

Fig. 5. HEIGHTS calculations of He pumping coefficient as a function of Li velocity at 10-keV incident particle energy.

4. Summary of particle pumping

To pump He at the minimum required rate of about 4–5% of impinging current, one needs a He diffusion coefficient $<10^{-8}$ m^2/s for reasonable liquid velocities. Recent studies suggest that such diffusion values may be feasible. Other mechanisms to enhance particle pumping due to internal flows as a result of magnetohydrodynamics (MHD) were recently suggested. Because the He penetration depth is only several monolayers, the MHD enhancement is not achievable for several reasons. First, the internal flow is not inward but circular; thus, the average time of the implanted particle spent near the surface is about the same or more without the internal flows, which may actually enhance the release rate. More important, even assuming an inward velocity of 1 m/s as suggested by some authors, one should realize that the liquid is moving with velocities of 10–20 m/s, so the resultant velocity is still mainly in the flow direction. A more important trapping mechanism, suggested by the present author, is bubble formation in the near implantation region. These bubbles (if developed) will trap helium, deuterium, and tritium and effectively enhance the pumping ratio.

Analytical and numerical models were developed in this work to study helium and hydrogen entrapment in the moving liquid metal surfaces. The analytical model offers a quick assessment of He removal efficiency as a function of system parameters of the incident He particles and the flowing liquid–metal surface. For similar system parameters both models yield, to the first order, similar values of He pumping coefficient. The integrated numerical model is more general, with a wide range of applications and different conditions. The numerical model, which takes into account an accurate spatial profile of particle implantation, the temperature dependence of material properties, and different boundary conditions calculates more precise values for particle entrapment in liquid surfaces.

The HEIGHTS numerical calculations also indicate that deuterium and tritium particles will be completely pumped by the flowing Li. This is because of the low molecular recombination coefficient of hydrogen isotopes. Hydrogen isotopes cannot leave the surface in the atomic form. Higher recombination coefficients require a large concentration flux at the surface. This is not achieved due to the liquid motion.

Because of several uncertainties, more data are needed on He diffusion and trapping, such as bubble formation and growth in liquids that could significantly alter the kinetics of particle recycling at the liquid surface. For example, bubble formation, growth, and bursting will cause liquid splashing that will detrap He and DT particles. Liquid splashing or macroscopic ejection of liquid droplets can significantly degrade the plasma behavior in the SOL and seriously contaminate the main plasma, leading to disruptions. Therefore, one needs to consider in detail the synergistic effects of He/D/T interactions with moving liquids and the consequences of droplet formation and behavior of the SOL plasma.

Acknowledgements

Work is supported by the US Department of Energy, Office of Fusion Energy Science, under Contract W-31-109-Eng-38.

References

[1] J.N. Brooks, T.D. Rognlien, D.N. Ruzic, J.P. Allain, J. Nucl. Mater. 290–293 (2001) 185.
[2] A. Hassanein, I. Konkashbaev, J. Nucl. Mater. 273 (1999) 326.
[3] T. Ronglien, 2001, personal communication.
[4] K.L. Wilson, Nucl. Fusion 1 (1984) Chapter 3 (Special Issue).
[5] M.A. Pick, K. Sonnenberg, J. Nucl. Mater. 131 (1985) 208.
[6] M.I. Baskes, J. Nucl. Mater. 92 (1980) 318.
[7] A. Hassanein, J. Nucl. Instrum. and Meth. Phys. Res. B13 (1985) 225.
[8] A. Hassanein, B. Wiechers, I. Konkashbaev, J. Nucl. Mater. 258–263 (1998) 295.
[9] A. Hassanein, J. Nucl. Mater. 233–237 (1996) 1547.